Surface Optical Mode in Semiconductor Nanowires

S. Dhara, Prasana Sahoo, A. K. Tyagi and Baldev Raj
Surface and Nanoscience Division,
Indira Gandhi Center for Atomic Research, Kalapkkam,
India

1. Introduction

Semiconducting nanowires represent interesting solid state systems with unique geometry offering great possibility for further development of optoelectronic devices and sensors applications with numerous possibilities for studying exciting physical phenomena arising from carrier confinement and the large surface-to-volume ratio (Hayden 2008, Pauzauskie & Yang, 2006; Yang et al., 2010; Lu & Leiber, 2007; Patolsky et al., 2007; Cao et al., 2009; Algra et al., 2008 & Wang et al., 2001). However, the growth of nanowires free of contaminants, controlled surface states and structural defects is still one of the key issues.

Studies comparing Raman scattering experiments of bulk and nanostructured materials have been reported in literature for several different kind of systems with extensive use as a primary characterization tool for study of phase and optical properties of nanowires and nanoparticles. (Zeng et al., 2006; Lin et al., 2003; Mahan et al., 2003; Adu et al., 2006; Hartschuh et al., 2003; Zardo et al., 2009; Cao et al., 2006; Shan et al., 2006; Pauzauskie et al., 2005; Xiong et al., 2006).With respect to one-dimensional (1-D) structures, several new phenomena have been reported to date, e.g., the high surface-to-volume ratio enabling the measurement of surface optical (SO) phonon modes (Gupta et al., 2003; Xiong et al., 2004; Spirkoska et al., 2008; Sahoo et al., 2009a; Sahoo et al., 2010; Adu et al., 2006). A increase in the scattered intensity is reported for nanoscale structures with respect to their bulk counterpart, describing the effect denominated as 'Raman antenna effect' (Xiong et al., 2004; Xiong et al., 2006; Cao et al., 2007). In addition, polarization dependent experiments on single carbon nanotubes and nanowires have shown that the physics behind Raman scattering of such 1-D nanostructures can differ significantly from the bulk (Frechette et al., 2006; Pauzauskie et al., 2005; Livneh et al., 2006; Cao et al., 2006). As a matter of fact, the highly anisotropic shape of the nanowires can lead to angular dependencies of the phonon modes which otherwise would not be expected from selection rules (Pauzauskie et al., 2005; Nobile et al., 2007). In general, Raman spectroscopy is an efficient tool to provide qualitative information from semiconductor by probing SO modes.

1.1 Surface optical phonons

SO phonons are similar in concept to bulk phonons, except that the atomic amplitudes are confined to the near-surface region of the material. The amplitudes of these phonons decay exponentially with distance measured away from the sample SO modes. In general, two

different types of SO phonon modes, depending on the penetration depths, can be distinguished as macroscopic and microscopic ones. Macroscopic SO modes are classified as optical (e.g. Fuchs-Kliewer; Fuchs & Kliewer, 1965) and acoustic (e.g. Rayleigh) SO phonon frequencies. Acoustic SO modes in isotropic elastic media propagate along the surface or interface with displacements in the sagittal plane which is defined by the normal to the surface and the direction of propagation (Wallis, 1994). These modes decay exponentially into the bulk and the penetration depth is proportional to the wavelength in the long-wave limit. Contrary to an acoustic mode the Fuchs-Kliewer phonon is connected to a macroscopic electric field (Fuchs & Kliewer, 1965). The frequency of a Fuchs-Kliewer phonon can be determined by solving the Laplace equation for the electrostatic potential of an ionic crystal under appropriate electromagnetic boundary conditions. Then the frequency is found to lie in between the frequency of the transverse optical (TO) and longitudinal optical (LO) bulk phonon. The corresponding pictorial representation of the atomic motion in a phonon mode has been illustrated in figure 1 (Richter et al., 2000).
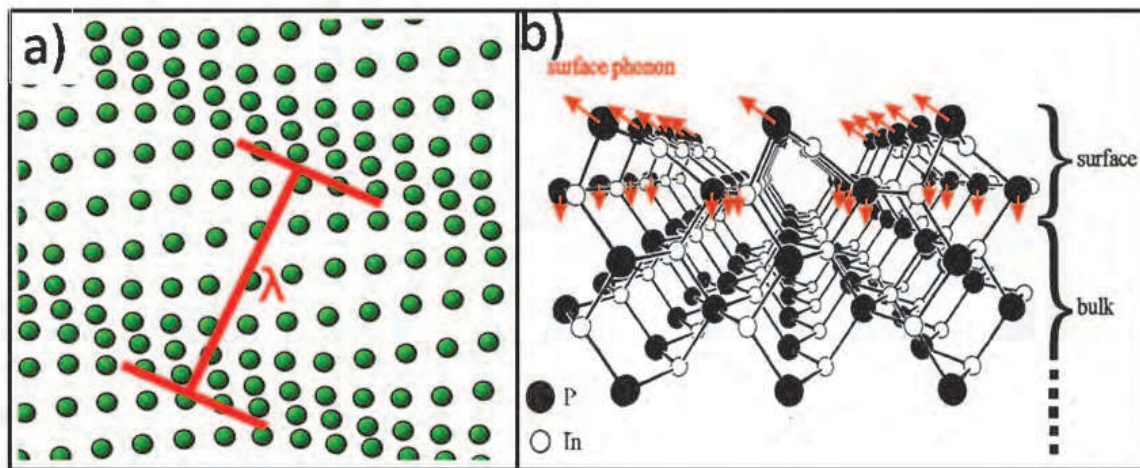

Fig. 1. Schematic representation of the a) atomic motion in a phonon mode (http://en.wikipedia.org/wiki/Surface_phonon) and b) SO phonon. The atomic displacements of SO phonons are confined to the top atomic layers. The atomic positions and the eigenvector in this example correspond to the higher frequency gap mode (270 cm^{-1}) of InP (110) at point $\bar{\Gamma}$ in the SO Brillouin Zone. (Richter, et al., 2000 Copyright © Xiamen University Press).

Experimental techniques for analyzing SO phonon properties have so far been based on SO phonon sensitive probes such as low-energy electrons and atoms, i.e. high resolution electron energy loss spectroscopy and He-atom scattering (Ibach & Mills, 1982; Benedek & Toennies, 1994). Due to the strong interaction of low-energy electrons and atoms with matter, the penetration depth of these probes is limited to the few outermost atomic layers giving rise to the sensitivity of SO modes in these techniques. Raman spectroscopy, in contrast, is based on the comparably weak interaction of photons with matter. Even under strong absorbing conditions the penetration depth of photons is no less than approximately fifty atomic layers and thus the Raman signal is bulk rather than SO mode related. However, the resolution and sensitivity of modern Raman equipment allows also for the observation of Raman signals generated by SO phonons (Gupta et al., 2003; Xiong et al., 2004). The reasons are, firstly the vibrational frequencies of SO phonons are different from those of the

bulk, since the top layer is free and bonding atoms are missing. Secondly, the energies of electronic states corresponding to the surface are different from bulk states and thus the resonance condition of SO phonons is different from that of bulk phonons. These differences in SO and bulk phonon scattering are pronounced for a perturbed surface or for hetero-termination i.e., when a surface is terminated with atoms not being present in the bulk.

SO phonons are reported in polar semiconductors exhibiting a formal charge separation between cation and anion sub-lattices. These SO modes show dispersion, i.e. their frequency depends on the wave vector q measured along the surface. For any q vector, the SO mode frequency ω_{SO} lies between those of the $q = 0$, LO and TO phonons. The SO phonon dispersion depends both on the dielectric function of the semiconductor as well as on the material, e.g. air, oxide, or liquid in contact with the surface. Wherever there is an interface between different materials with different dielectric functions, generally, there will be interface modes. They are solutions to Maxwell's equations with appropriate boundary conditions (Sernelius, 2001). These modes, which are localized to the interface, can propagate along the interface.

Normally, SO modes are observed when the translational symmetry of the SO potential is broken. This break down of symmetry can activate a larger wave vector SO mode whose frequency is sufficiently separated from the other Raman-active optical phonons, to be observed experimentally. An interplay of a strong Fourier component of the perturbed SO potential acts as a source of wave vector supplied by the symmetry breaking (Sernelius 2001). This can be achieved in several ways, e.g., by surface roughness, or by formation of a grating along the surface. Another method for detecting SO modes involves placing a prism at the surface of the sample. The evanescent wave from the prism–sample interface can probe the surface and the desired SO mode (Falge et al., 1974)

Overall, Raman spectroscopy of nanostructures represents an extremely active and exciting field for the benefit of science and technology at the nanoscale. The arising new phenomena and technical possibilities not only open new vistas for the characterization of materials but also for the understanding of fundamental processes at nanoscale. In this chapter, we provide a review of SO modes on nanowires using Raman spectroscopy depicting overview of the appearance of new modes and their effect on geometry of samples.

2. Surface optical phonons from semiconductor nanowires

There are geometry and size-related phonons appearing for several different kind of systems when dealing generally with nanowires and nanoparticles, such as the SO and breathing modes arising from acoustic confinement. In case of nanowires, the geometry is one of the long filaments. The cross-sectional shape of nanowire matters for the SO phonon dispersion. It is usually observed that the TO and the LO modes have a position in energy close to that observed in bulk. When scaling down the size and the dimensionality of the structures, the position can change along with the appearance of new Raman modes due to breakdown of translational symmetry in the finite size. Moreover, effects related to the shape of the system can become significant. The existence of boundary conditions at the nanoscale gives rise to electric and polarization forces. The surface represents a new mechanical boundary, since the surface atoms are less bound and experience a different local field than that from the bulk. This has consequences even in the propagation of an optical phonon.

Several works have reported the presence SO modes in Raman spectra of semiconductor nanowires which have been assigned to SO phonons (Gupta et al., 2003; Shan et al., 2006; Sahoo et al., 2008a, 2010b; Sahoo et al., 2010; Lin et al., 2003; Zeng et al., 2006; Spirkoska et al.,

2008). The SO phonons are generated at the interface between different materials with different dielectric functions and propagate along the interface. The atoms involved in their propagation are those close to the surface, so that the amplitude of the oscillations decays exponentially with the distance from the surface. This mode is activated by breakdown of the translational symmetry of the SO potential, which in the case of the nanowire can be addressed to the presence of roughness, saw tooth faceting on the nanowire sidewall or to a diameter oscillation along the nanowire length. There are two characteristics which are distinctive of the SO modes and can therefore allow a reliable assignment of the mode: the dependence of the phonon frequency (1) on the dielectric constant of the medium surrounding the wires and (2) on the diameter or on the period of the diameter oscillation of the wires. Indeed, it was already observed that blue shift of the SO mode value increases with the dielectric constant of the surrounding optical medium and decreases with the nanowire diameter (Gupta et al., 2003; Sahoo et al., 2009). Furthermore, the frequency of the SO modes at the center of the Brillouin zone is located between those of the TO and the LO and also the long-wavelength ($q = 0$) SO modes are hard to identify experimentally, as they strongly overlap with the TO ($q = 0$) phonon.

2.1 SO phonons in cylindrical geometry

The SO modes dispersion at the interface between a semiconductor and a dielectric material can be calculated taking into account of the geometrical constraint and surrounding dielectric medium, by imposing the condition:

$$\varepsilon(\omega) + \varepsilon_m = 0 \tag{1}$$

where $\varepsilon(\omega)$ the dielectric function of the semiconductor and ε_m is the dielectric constant of the medium. For a cylindrical interface, the SO mode frequency can be obtained by solving the following equation,

$$\varepsilon(\omega) + \epsilon_m f(qr) = 0 \tag{2}$$

where r is the radius of the cylinder, and

$$f(x) = \frac{I_0(x)K_1(x)}{I_1(x)K_0(x)}, \tag{3}$$

where I and K are Bessel functions and $x = qr$. For an interface between a dielectric medium and a semiconductor surface, on solving (1) with the dielectric function

$$\varepsilon(\omega) = \varepsilon_\infty + \frac{\varepsilon_0 - \varepsilon_\infty}{1 - \frac{\omega^2}{\omega_{TO}^2}} \tag{4}$$

for a semiconductor, the SO mode frequency is

$$\omega_{SO} = \omega_{TO}\sqrt{\frac{\varepsilon_0 + \varepsilon_m}{\varepsilon_\infty + \varepsilon_m}}, \tag{5}$$

where ε_0 and ε_∞ are the static and high-frequency dielectric constants, respectively. ω_{TO} is the TO mode frequency at zone center. This frequency is the asymptotic limit of the SO polariton, i.e. coupled SO phonons and photons.

$$\omega_{SO}^2 = \omega_{TO}^2 + \frac{\widetilde{\omega}_p^2}{\varepsilon_\infty + \varepsilon_m f(x)}, \quad x = qr, \tag{6}$$

where $\tilde{\omega}_p^2$ is the screened ion plasma frequency given by $\omega_{LO}^2 = \omega_{TO}^2 + \tilde{\omega}_p^2/\varepsilon_\infty$, ω_{LO} is the LO mode frequency at zone center, and $d = 2r$ is the wire diameter. For infinite-diameter cylinders, i.e. $r \rightarrow \infty$, $f(x) \rightarrow 1$,

$$\omega_{SO}^2 = \omega_{TO}^2 + \frac{\varepsilon_\infty(\omega_{LO}^2 - \omega_{TO}^2)}{\varepsilon_\infty + \varepsilon_m} \quad => \quad \omega_{SO} = \omega_{TO}\sqrt{\frac{\varepsilon_0 + \varepsilon_m}{\varepsilon_\infty + \varepsilon_m}}, \tag{7}$$

This is exactly the SO phonon frequency of an infinite semiconductor flat surface expressed by (5). Therefore, equations (6) and (7) establishes the dependency of the SO phonon energy on the external medium and on the size of the wire, since the position of the SO phonon can be related to the dielectric constant of the surrounding medium as well as to the nanowire radius. Furthermore, values of q for the activation of the SO mode can be determined experimentally (Gupta et al., 2003). Instead, the line width of the SO mode has not been yet well understood. The effect of the position of the SO modes can be evidently observed by comparing semiconductor nanowires with various diameters.

2.1.1 GaP nanowires

The SO potential along the axis of the GaP nanowire is perturbed by a strong component with wave vector q (Gupta et al., 2003). Thus, inelastic light scattering via SO phonons with this average wave vector is particularly important. The wave vector q, responsible for the observation of the SO band, can be deduced by comparing the computed SO frequencies $\omega_{SO}(q)$ to those obtained experimentally.

Figure 2 shows the Raman spectra of the optical phonons for GaP nanowires with diameter of 50 nm in air ($\varepsilon_m = 1$), dichloromethane ($\varepsilon_m = 2$), and aniline ($\varepsilon_m = 2.56$).
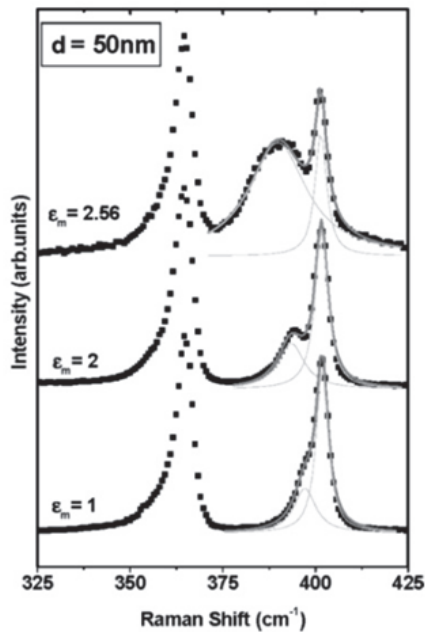

Fig. 2. Raman spectra of GaP nanowires with diameter $d= 50$ nm recorded in three different media with different dielectric constant (ε_m). The low, middle and high frequency bands are identified respectively with the TO, SO, and LO phonons. The solid lines represent Lorentzian line shapes used to fit the SO and LO band. (Gupta et al., 2003 Copyright © American Chemical Society; Applied for permission).

It is assumed that the LO and TO phonon branches are dispersion less as shown by horizontal lines. The nanowire diameter is given by $2r$, and the thin lines are the result of a Lorentzian line shape analysis. The decomposition of the band into individual Lorentzians is also shown. The lowest and highest frequency bands, respectively, are identified with the first-order modes of TO at 367 cm^{-1} and LO at 401 cm^{-1}. A third Raman band lies midway between the TO and LO bands (Fig. 2). This band is assigned to SO modes because of its sensitivity to the dielectric constant of an external medium (ε_m) e.g. air, dichloromethane, and aniline in contact with the nanowire. The SO band show red shift (Fig. 2), as the dielectric constant of the surrounding medium is increased. The peak positions of the LO and TO bands, however, do not change. Based on this observation, the intermediate frequency band has been unambiguously assigned to SO modes.
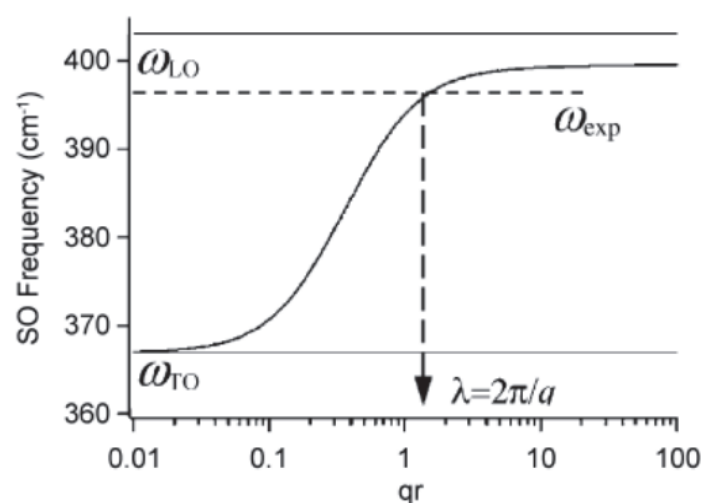

Fig. 3. Calculated dispersion of the SO mode for a GaP nanowire (ε_m =1). The arrow indicate the q= 0, LO and TO phonon frequencies. (Gupta et al., 2003 Copyright © American Chemical Society; Applied for permission).

From the calculated SO dispersion and the ω_{SO} obtained from experiments with the nanowires in various dielectric media (e.g. the crossing points between the solid curve and the dashed lines in Fig. 3), the wavelength $\lambda = 2\pi/q$ of the SO potential (perturbation) which is important for activating the SO mode scattering has been estimated. For cylindrical cross section GaP nanowires, $\lambda = 2\pi/q$ is ~ 40 nm. In case of d= 20 nm wire, the maximum dispersion takes place at q^* wire ~ 2 ×10^7/m by using equation (6). The q^* value marking maximum dispersion is much larger than its counterpart for SO modes at a plane surface (i.e., $q_{plane} \sim \omega_{LO}/c$ =2.5× 10^5/m). Thus, it is clearly important to use the correct (cylindrical) geometry while describing the SO phonons in small diameter nanowires (Adu et al., 2006; Spirkoska et al., 2008).

It appears that values of the SO band frequency, as calculated for x= 4, correspond to the experimentally obtained values for the sample of d= 50 nm, while x= 1.5 values are close to those SO mode observed for the sample with a diameter, d= 20 nm. Approximately the same value of $q = 1.5\times 10^8$/m is found for the two sets of wires d= 20 or 50 nm. Therefore, the length scale which is responsible for excitation of the SO mode is given by $2\pi/q$ = 40 nm. Since this length scale is similar in both cases, there must be an inherent length scale in the nanowires responsible for the activation and observation of the SO band. The symmetry

breakdown mechanism responsible for the observation of the SO band is due to the presence of the wire diameter modulation along the nanowire growth direction. This modulation can indeed be observed in TEM images (Fig. 4) where it has been shown that four different images with different wire diameters with modulation wavelength λ. The diameter modulation wavelengths, λ ($\approx$ 30-70 nm), for the small subset of nanowires (Fig. 4) is consistent with the length scale ($\approx$ 40 nm).
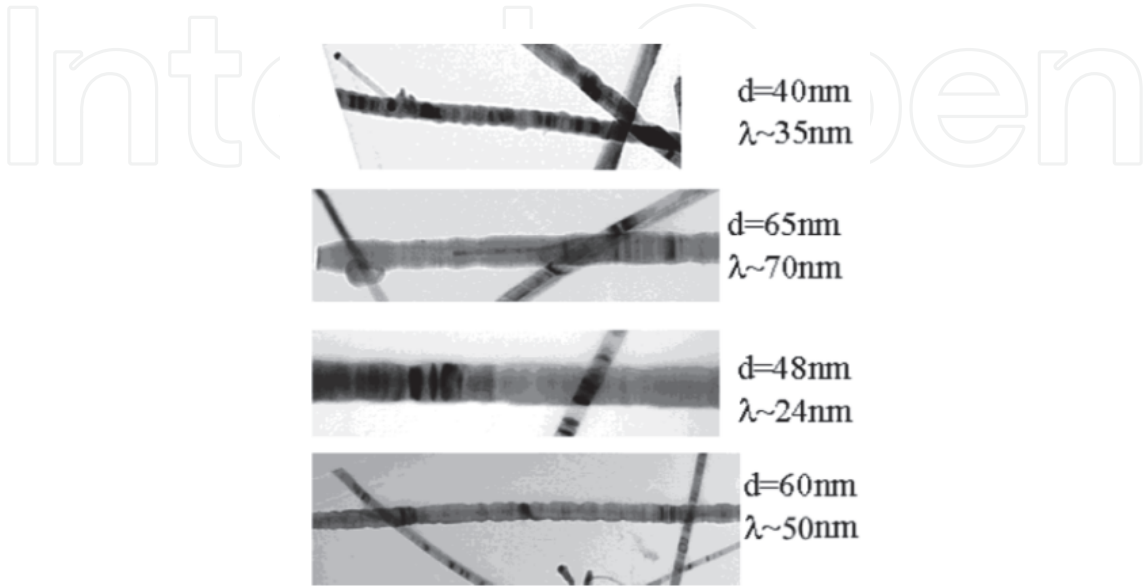

Fig. 4. Bright field TEM images of GaP nanowires showing nearly periodic modulation of wire diameter. The diameter and the modulation wavelength for each image appear to the right. Diameter oscillations have been reported to be more prominent in larger diameter nanowires. (Gupta et al., 2003 Copyright © American Chemical Society; Applied for permission).
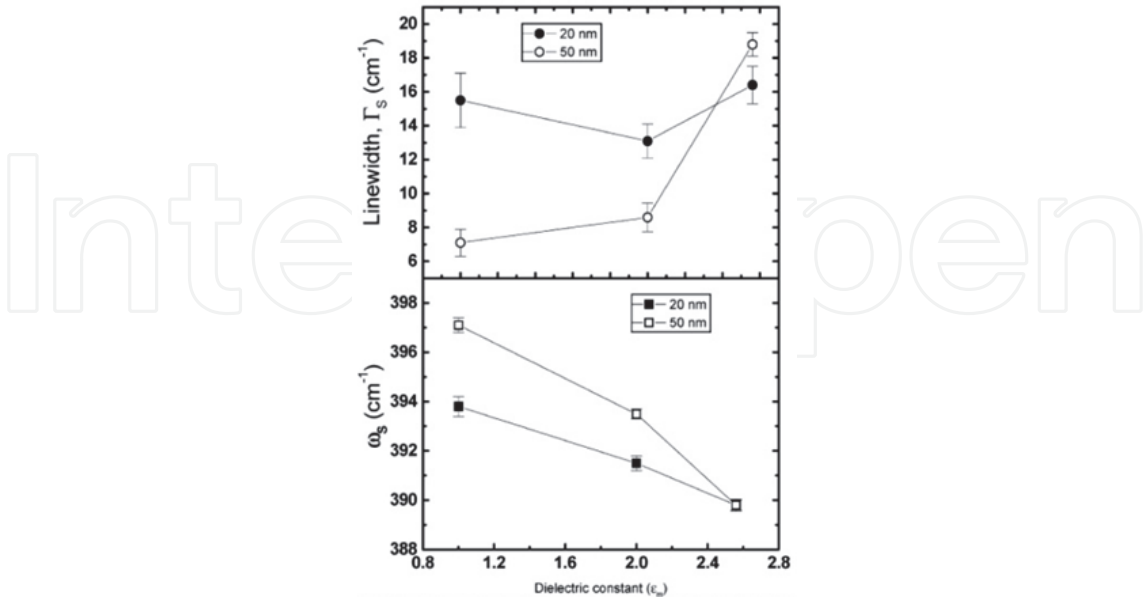

Fig. 5. Variation of the line shape parameters for the SO band (peak position and line width) as a function of the dielectric constant of the overlaying medium. (Gupta et al., 2003, Copyright © American Chemical Society; Applied for permission).

Again, it is already discussed that the dispersion for a SO mode calculated in a cylindrical geometry is crucial for estimating the wavelength of the important Fourier component of the SO potential that breaks the symmetry and "activates" the SO modes in a Raman scattering event. It is also possible that SO Raman mode from larger nanowire diameters ($d > 40$ nm) in the lognormal diameter distribution with a more prominent diameter modulation (Fig. 5) might dominate the SO spectrum for the nanowire ensemble. This assumption can be proved if SO mode frequency can be measured from individual wires with known diameter modulation wavelength.

The SO band position does not include any dynamics of the SO phonons, and therefore it is inadequate to describe the variation of the SO mode line width as a function of ε_m as shown in figure 5 (top). The line width measured in air for the SO band in the 20 nm diameter sample is twice of that observed in the 50 nm sample, even if the line widths of the LO mode in the two nanowire samples with different diameter distributions are comparable to within 10% in all overlaying media. This implies that the SO modes in the 20 nm nanowires have a lifetime that is half of the 50 nm nanowire batch. This may results due to the difference in the decay channel phase space available to the SO phonons for the two samples as the dielectric constant varies.

2.1.2 GaAs nanowires

Figure 6 represents scanning electron microscopy image of the GaAs nanowires, grown by molecular beam epitaxy (Spirkoska et al., 2008). The Raman spectra have been recorded in ensembles of GaAs nanowires having diameters 160 and 69 nm (Fig. 7a). The existence of a SO mode is confirmed by comparing the spectra of the nanowires in an environment of air and PMMA with higher value of dielectric constant. As expected, the SO mode shifts to lower wave numbers for smaller diameters, as it is observed in the spectra obtained for nanowires with an average diameter of 69 nm. The entire trend of the position as a function of the diameter is shown in figure 7b. The SO mode is barely observed as the position is very close to the LO phonon for the nanowire with the largest diameter. Continuous line indicates data for nanowires with a circular section. GaAs nanowires exhibit a hexagonal section explaining the discrepancy with the experimental data.
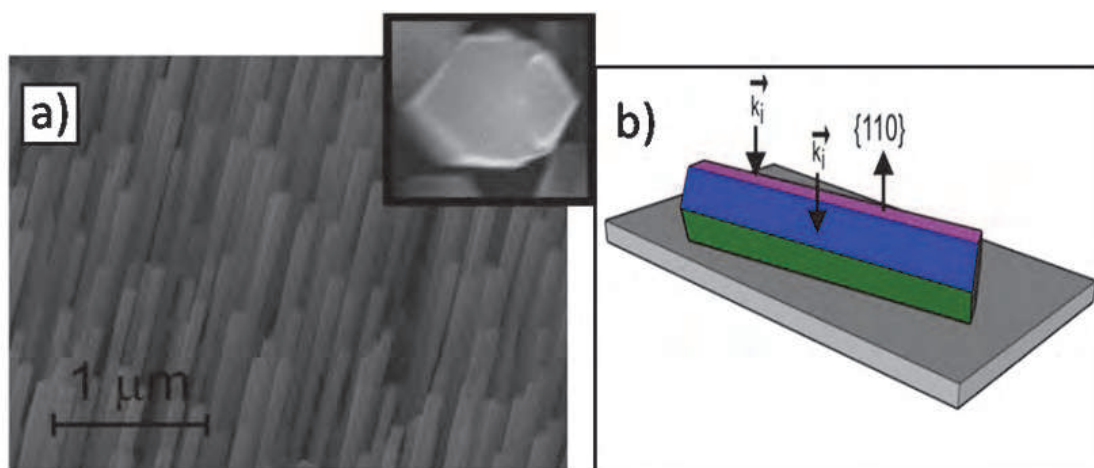

Fig. 6. a) Scanning electron micrograph from the as-grown GaAs nanowires. The hexagonal cross section of the nanowires is presented in the inset. b) Schematic drawing of the scattering geometry of the measurements after transferred of the GaAs nanowires onto Si substrate. (Spirkoska et al., 2008 Copyright © Institute of Physics.)
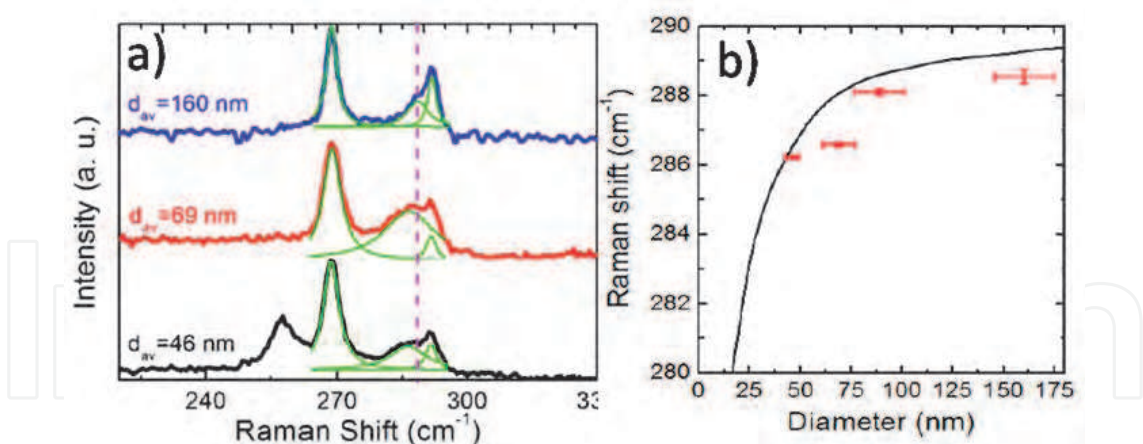
Fig. 7. a) Raman spectra of GaAs nanowire bundles with respectively an average diameter of 160 and 60 nm. The SO mode can be observed on the left of the LO mode in which the position of the SO phonon down-shifts with the decrease in diameter. b) Evolution of the SO phonon position as a function of the diameter of the nanowires. The line corresponds to the theoretical values expected for hexagonal cross section of GaAs nanowires. (Spirkoska et al., 2008 Copyright © Institute of Physics.)

2.1.3 GaN nanowires

In our latest study,(Sahoo et al., 2010) the SO phonon modes has been identified in GaN nanowires grown by vapor liquid solid (VLS) technique showing a strong correlation between the surface morphology and Raman phonon spectra. The SO phonons associated with A_1(TO) at 533 cm⁻¹ and E_1(TO) at 560 cm⁻¹ are calculated for GaN by taking the qr value of 1.07, which yields SO phonon frequencies (ω_{so}) pertaining to A_1 (654 cm⁻¹) and E_1 (688 cm⁻¹) characters (Fig. 8). Hence, the reported peaks around 652 and 691 cm⁻¹ has been accounted for SO phonon modes in GaN.
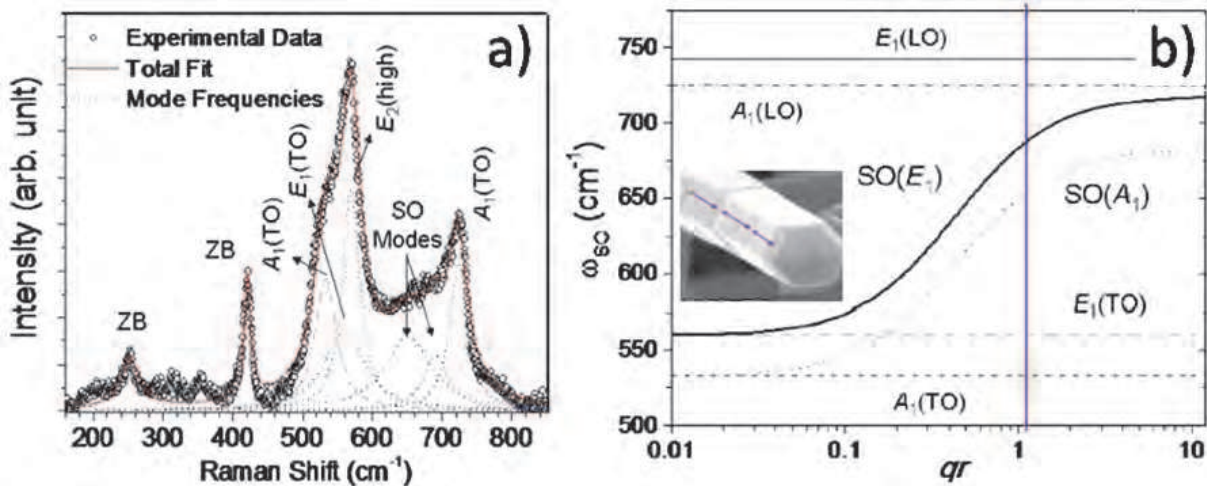

Fig. 8. a) Room-temperature Raman-scattering spectra of GaN nanowires showing the experimentally observed data and the Lorentzian fit for the individual peaks. b) Calculated SO phonon frequencies as a function of qr, full curve: SO(E_1), dashed curve: SO(A_1), horizontal lines are the LO and TO frequencies of E_1 and A_1 modes, as inscribed in the figure. Vertical dotted line is marked for $qr = 1.07$. Inset is a GaN nanowire with diameter modulation. (Sahoo et al., 2010 Copyright © Inderscience Enterprises Ltd.)

It can also be seen that the intensities of the observed SO phonons in the present study are comparable to other phonons. The magnitude of surface roughness determines the SO peak intensity owing to the breakdown of the translational symmetry of the SO potential. The wavelength $\lambda = 2\pi/q$ ($qr = 1.07$; $r \sim 250$) corresponding to the perturbation of SO potential has been estimated as ~1500 nm for the GaN nanostructures (using the dispersion relations in Fig. 8b for typical nanostructure diameter of ~500 nm). Surface roughness with a modulation of ~150–300 nm is observed (indicated by arrows in the inset of Fig. 8b) with any integral multiple equivalent to the λ (10×150 nm = 5×300 nm = 1500 nm) will be sufficient to initiate breakdown of translational symmetry in contributing SO potential toward SO modes. The process makes the intensity of the SO mode comparable to that of the other phonons.

SO mode in a single GaN nanowire grown by molecular beam epitaxy has also been reported by Hsiao and co-workers (Hsiao et al., 2007) during angle dependent Raman spectroscopy measurement with the z axis pointing along the crystallographic c axis of the rod. The direction of different angles between the laser polarization and the rod length (c axis) are shown in figure 9 (a). The reference frame (x, y polarization) is rotated against the rod. The angle between the laser polarization and the z axis (x axis) is represented by θ (φ) (Fig. 9a). In the Porto notation, (Arguello et al., 2969) the representations of $\theta = 0°$ and $\theta = 90°$ scattering configurations with $\varphi = 90°$ are x(z, z)$\bar{x}$ and x(y, y)$\bar{x}$, respectively. The hexagonal geometry shape with vibrational modes are resolved in $x(x+y, x+y)\bar{x}$ scattering configuration to obtain all main Raman peaks which further demands for application as angle selective nanosensors. However, a new peak at 708.5 cm^{-1} have been ascribed to the SO mode (Fig. 9b) which is absent in GaN compact film (also shown in lower spectra of figure 9b). With high surface-to-volume ratio and the high perfection of the hexagonal surface with highly crystalline structure, the peak is assigned to the SO mode of GaN nanocrystals rather than the disorder-active Raman mode which refers to the effect of defects in crystal or a-GaN and agrees well with the calculated value.
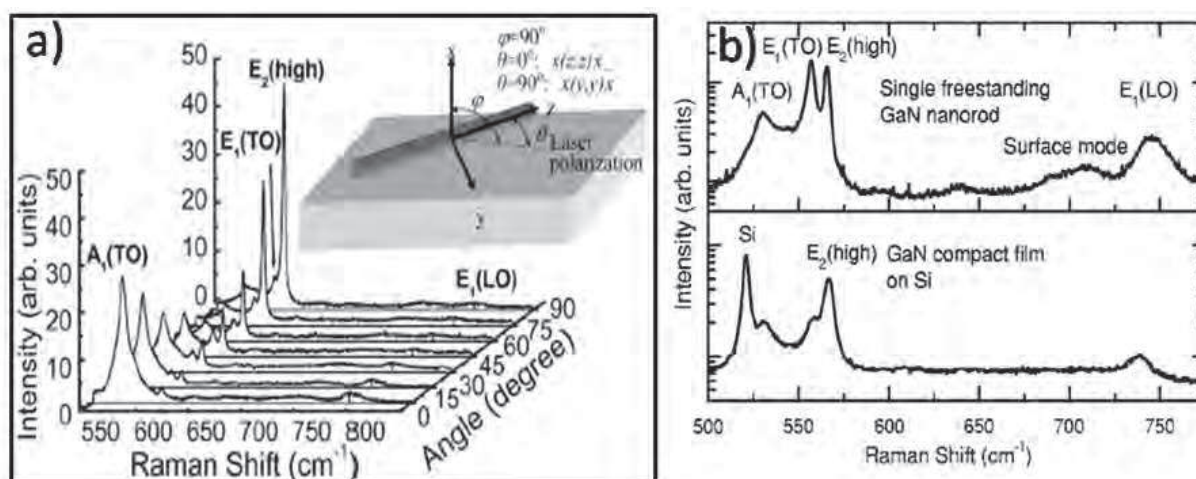

Fig. 9. a) Angle-dependent Raman spectroscopy measured at different angles between the laser polarization and the rod length (c axis). The inset shows a schematic diagram of the Raman scattering configurations measured on a single freestanding nanorod. b) Micro-Raman spectra measured from a single freestanding GaN nanorod and a compact GaN thin film. A prominent peak at 708.5 cm^{-1} is contributed from the SO vibrational mode of GaN nanorod. (Hsiao et al., 2007 Copyright © American Institute of Phys.)

2.1.4 InN nanowires

An optical mode of one-dimensional nanostructures of InN, such as nanowires and nanobelts grown by chemical vapor deposition, has been studied in our earliest report (Sahoo et al., 2008). Typical Raman spectra of nanowires and nanobelts are shown in figures 10(a) and (b), respectively and SO phonons modes have been reported taking into consideration of cylindrical geometry to both. The range of qr is determined from the dispersion relation of ω_{SO} as a function (Fig. 11a) by the spread in diameter ($d\sim 75$ to 150 nm for nanowires and ~ 50 to 200 nm for nanobelts). For $d=100$ nm the value of $qr = 1.18$ is shown as a vertical dot-dashed line in figure 11. Based on the above agreement the modes around 528–560 cm^{-1} have been assigned to SO modes with A_1 and E_1 characters, respectively. A further confirmation has been clearly reported by recording the spectra in a higher dielectric medium ($\varepsilon_m=2.24$ for CCl$_4$) which shows inherently a red shift of 4 cm^{-1} to SO modes. The spread in SO phonon essentially arises due to the wide range of diameter and dimension of the nanostructures.
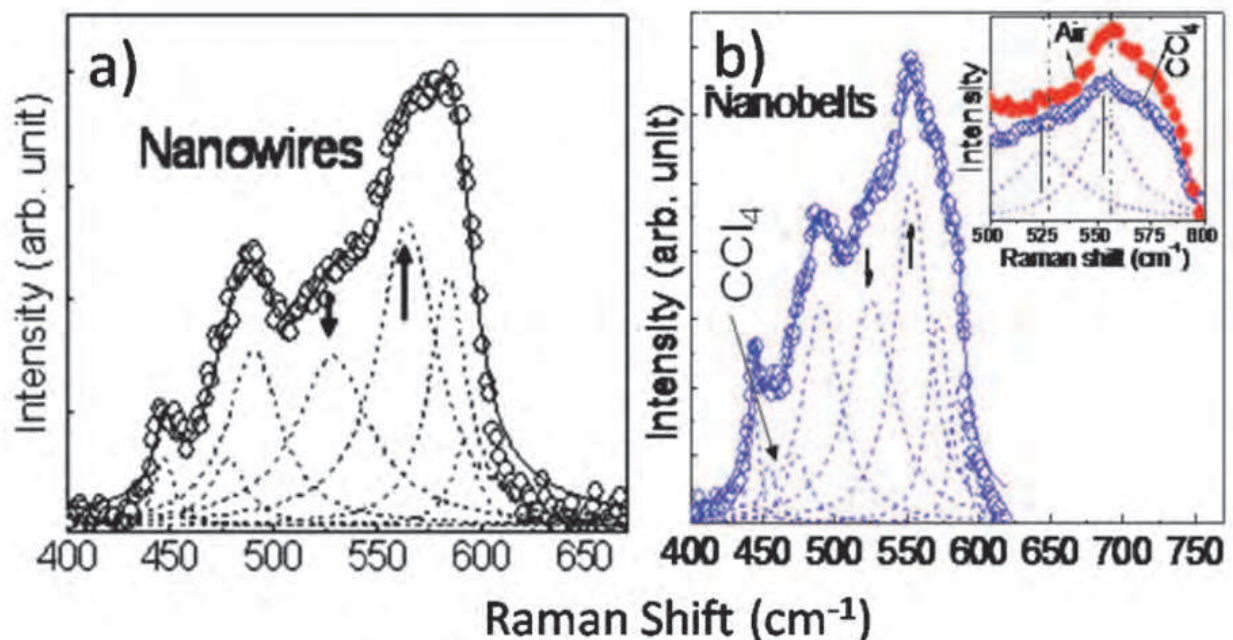

Fig. 10. Raman spectra for InN a) nanowires and b) nanobelts. Full curve: total fitted spectrum, dashed curves: individual fitted peaks. Peaks corresponding to SO mode are indicated by arrows. Raman spectra of InN nanobelts b) immersed in CCl$_4$. The inset shows SO modes under the expanded range of 500–600 cm^{-1}. (Sahoo et al., 2008 Copyright © American Institute of Physics.)

The wavelength $\lambda=2\pi/q$, corresponding to the SO potential, can be estimated as ~ 135 nm for nanowires and ~ 110 nm for nanobelts using the dispersion relations in figure 11 with maximum $qr=1.65$ for nanowires and~ 1.4 for nanobelts. Surface roughness with modulation of ~ 65 nm for nanowires (Fig. 11b) and ~ 55 nm for nanobelts in figure 11b have been observed. However, the intensity of SO modes found to be higher than that for the TO modes. Defects related to abrupt termination of translational symmetry in the nanostructures may reduce the intensities of fundamental phonon modes; on the other hand, rough surface and interface may result in intense SO modes.
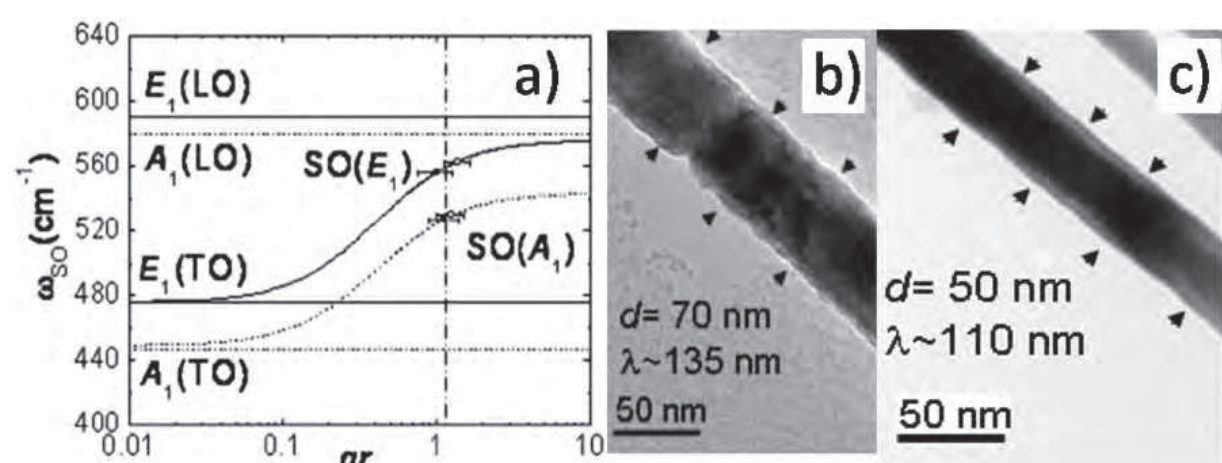
Fig. 11. a) Calculated SO phonon frequencies as a function of *qr*, full curve: SO (E_1), dashed curve: SO(A_1). Horizontal full and dashed lines are the TO and LO frequencies of E_1 and A_1 modes, respectively. Symbols are measured SO frequencies, open symbol: nanowires, filled symbol: nanobelts. Vertical line at *qr*=1.18 corresponds to d=100 nm. b) Surface roughness in typical nanowires and c) nanobelts. Arrows show the modulation in the surface structure. Diameters and the calculated wavelengths of SO potential are also inscribed. (Sahoo et al., 2008 Copyright © American Institute of Physics.)

2.1.5 AlN nanowires

In one of our recent studies (Sahoo et al., 2010) we have studied typical Raman spectra for optical phonons in AlN nanotips (Fig. 12a). Apart from the allowed optical phonons in AlN, an additional phonon mode at 850 cm^{-1} has been assigned to SO phonons, in view of its strong response to change in dielectric medium and good agreement with calculated SO phonon frequency. A prominent red shift of SO mode (23 cm^{-1} in CCl$_4$ medium) has been reported (inset of Fig. 12a).
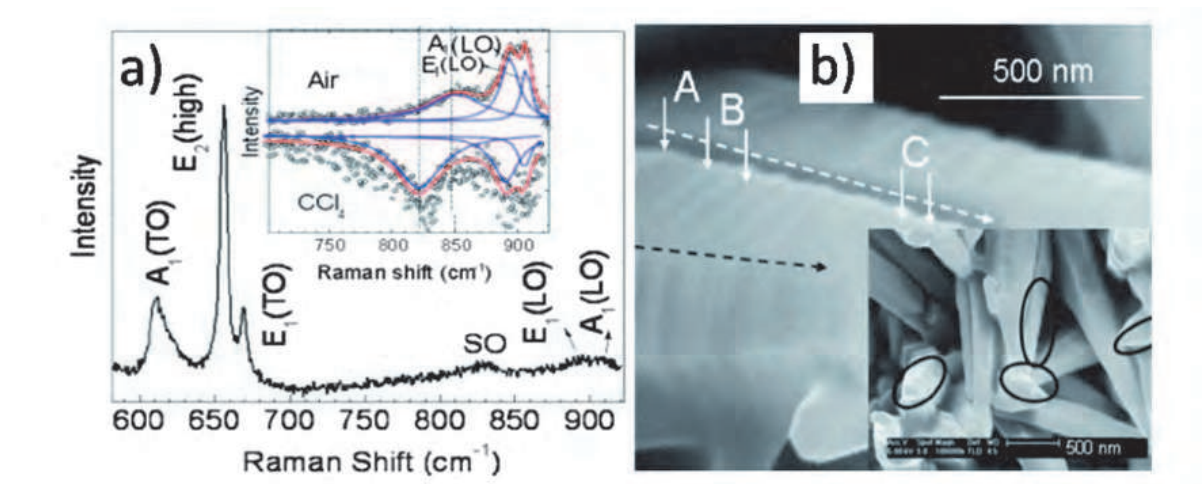

Fig. 12. a) Raman spectra of AlN nanotips recorded in CCl$_4$. Inset shows comparison of the position of SO phonon peak in air and CCl$_4$ medium, b) Morphological study at high resolution FESEM image of AlN nanotips with arrows showing the modulation of the surface. Inset shows corresponding marked region with distinct surface modulation. (Sahoo et al., 2010 Copyright © American Institute of Physics.)

The typical analysis of the nanotip surface (as directed by two doted arrows) shows that the steps (labeled as A, B, and C in Fig. 12b) are systematically decreasing along the growth direction. The width ($d=2r$) of the steps are 120, 90, and 50 nm with a corresponding length of 350, 260, and 140 nm, respectively. The wavelengths ($\lambda=2\pi/q$) of perturbation have been calculated taking into account of the corresponding r and $x=1.2$ value of each step. The values of wavelength corresponding to A, B, and C are reported to be 314, 235, and 130 nm, respectively. Thus these perturbation values, which are in close agreement with the length of the steps (Fig. 12b), absorb the required phonon momentum for the observation of the SO mode.

2.1.6 InGaN/GaN multi-quantum-well nanopillars

In another study (Wu et al,. 2009) we have reported the fabrication and the observation of SO phonon in aligned GaN nanopillars with spatial control of embedded InGaN/GaN multi-quantum-well (MQWs) using focused ion beam milling. Figure 13 (a) shows the SEM image of resulting InGaN/GaN MQWs structure milled with a serpentine-scanning beam and subsequently wet-etched with KOH solution. The pillar base diameter (Fig. 13a) is around 95 nm with aspect ratio of 7: 1. The pillar size is further reduced to 30 nm with enhanced high aspect ratio of 16: 1, with an extended KOH treatment time. The presence of surface roughness or even surface modulations of ~ 25 nm at two different regions of these 1-D MQW nanopillars have been observed (Fig. 13b).
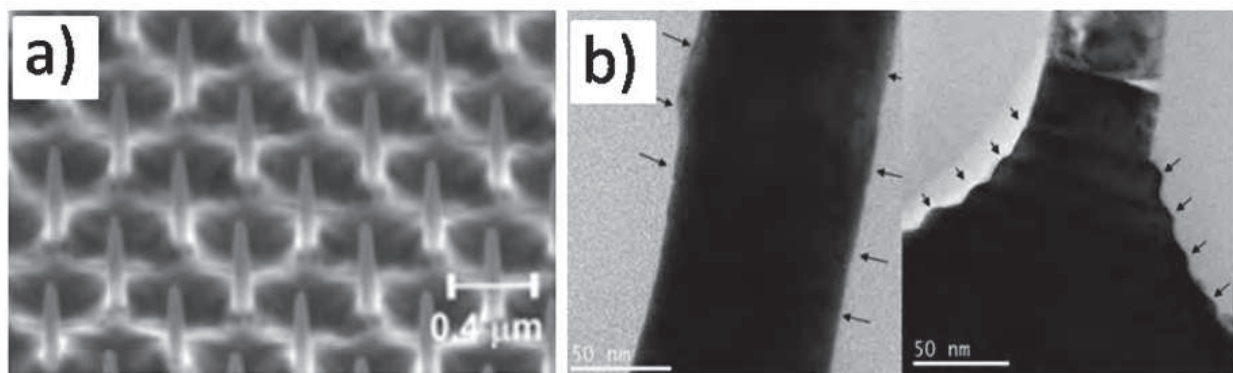

Fig. 13. a) SEM tilted-view images showing FIB milled nanopillars after KOH treatment.
b) Surface roughness in typical MQW nanopillars. Arrows show the modulation in the surface structure at two different regions. (Wu et al., 2009 Copyright © John Wiley & Sons, Ltd.)

Figure 14 displays distinct Raman features of KOH etched nanopillars with 632.8 nm (Fig. 14a) and 514 nm (Fig. 14b) laser excitations. Along with all allowed Raman modes, the fitted broad peak in the range 665–699 cm^{-1} (inset in Fig. 14b) have been examined carefully to elucidate the possibility of SO phonon being responsible. The Raman spectra for nanopillars in a higher dielectric medium ($\varepsilon_m = 2.56$ for aniline) have been recorded and compared with those in air for the same excitation of 532 nm laser line (Fig.15a). It is reported that the peak positions of the $A_1(LO)_{GaN}$ and $A_1(LO)_{InGaN}$ modes did not change, whereas an apparent red shift of ~15 cm^{-1} for SO modes for GaN has been reported for the spectrum collected from the sample surrounded with a higher value of dielectric constant than that of air ($\varepsilon_m = 1$). These unidentified peaks had been assigned to SO phonon modes originating from surface roughness or even surface modulation in 1-D MQW a nanopillars (Fig. 13b).
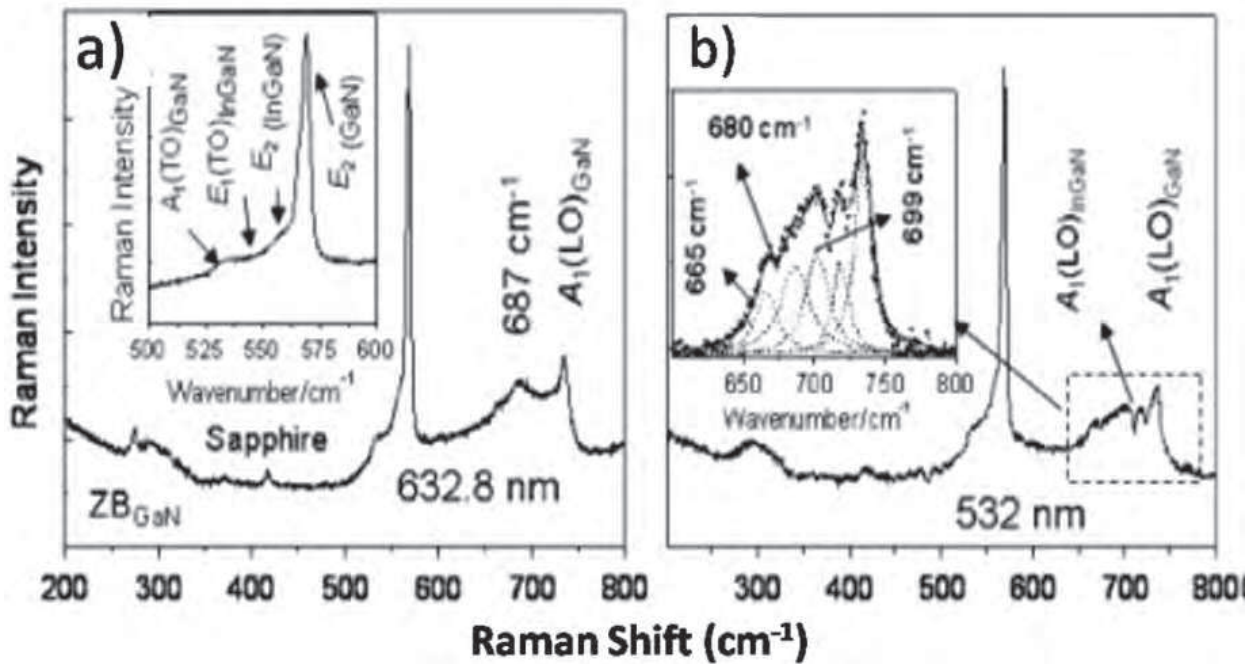
Fig. 14. Spectra for wet chemical (KOH) etched nanopillars with the excitations of (a) 632.8 nm, with inset showing the detailed spectrum in the 500–600 cm^{-1} range and (b) 532 nm laser lines with inset showing the Lorentzian fits for multiple peaks in the 625–775 cm^{-1} range. (Wu et al., 2009 Copyright © John Wiley & Sons, Ltd.)

The plots of ω_{SO} for GaN as a function of qr dispersion relation of SO modes for these 1-D MQW nanopillars, taking into consideration of cylindrical geometry, is shown in figure 15b.
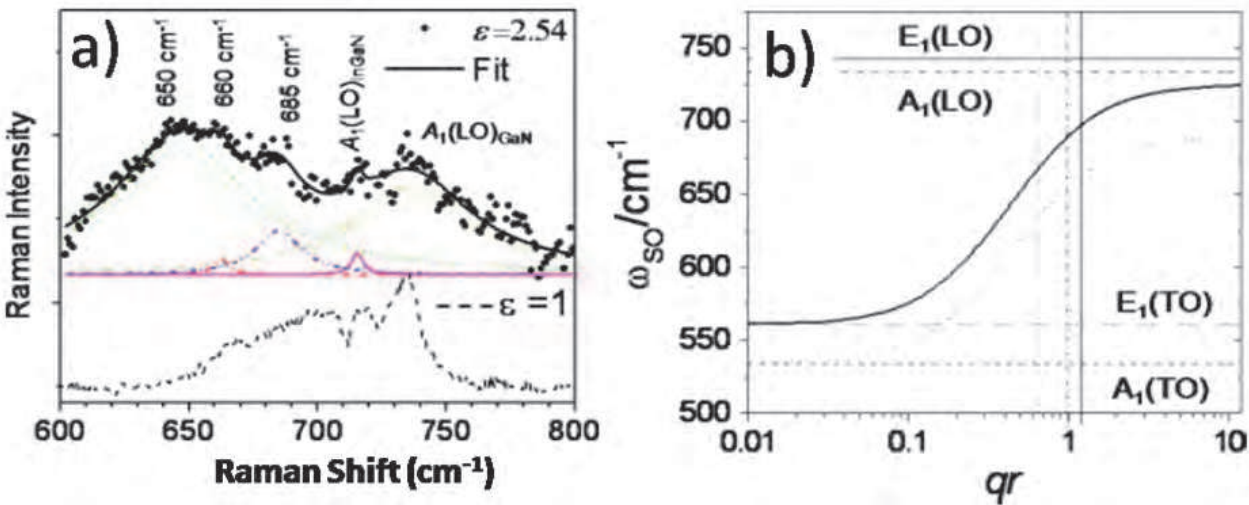

Fig. 15. a) Raman spectra for wet-etched nanopillars immersed in aniline (ε = 2.54) and in air (ε = 1) with the excitation of the 532 nm laser line. Lorentzian fits for multiple peaks are also shown for the spectrum recorded with aniline. b) Calculated SO phonon modes of GaN as a function of qr: full curve, SO(E_1); dashed curve, SO(A_1); horizontal full and dashed lines are the TO and LO wavenumbers of E_1 and A_1 modes, respectively. Vertical lines are marked for qr = 0.64 (dotted), qr = 0.99 (dash-dotted), and qr = 1.18. (Wu et al., 2008 Copyright © John Wiley & Sons, Ltd.)

The wavelength $\lambda = 2\pi/q$, corresponding to the SO potential (perturbation), has been estimated as ~250–300 nm for the nanopillars (using the dispersion relations in Fig. 15b with various excitations). Surface roughness with a modulation of~25 nm is observed (Fig. 14b) in these nanostructures. Modulation length with any integral multiple equivalent to the λ (10×25 nm=250 nm or 12×25 nm=300 nm) will be sufficient to initiate breakdown of translational symmetry for the contribution of the SO potential towards the SO phonons and to make the intensity of the SO modes comparable to that of other phonons. The origin of the broad new peak in the range of 665–699 cm^{-1} can be assigned to the SO modes corresponding to 1-D GaN and In$_{0.15}$Ga$_{0.85}$N.

2.2 SO phonons in rectangular geometry

The theoretical prediction for the SO modes varies from circular cross section wires to rectangular. However, there is no analytical expression for SO modes in rectangular cross section wires. Nevertheless, the dielectric continuum (DC) model approach that has been used for cylindrical nanowires remains the most elegant method and provides analytical expressions for $\omega_{SO}(q)$ vs ε_m for rectangular wires with further approximation,. An approximate DC model for rectangular wires has been introduced by Stroscio and co-workers (Stroscio et al,. 1990; Stroscio et al., 2001) that neglects the exponentially decaying electrostatic fields emanating from the corner regions. This assumption makes the problem separable in the plane perpendicular to the wire axis. The following dispersion relations is obtained for the SO phonons upon imposition of the usual electrostatic boundary conditions;

$$\epsilon_w(\omega)\tanh(q_i L_i/2) + \epsilon_m = 0, \tag{8a}$$

$$\epsilon_w(\omega)\coth(q_i L_i/2) + \epsilon_m = 0, \tag{8b}$$

Equation 8a is the symmetric (S) mode and equation 8b is the asymmetric (AS) mode, $\varepsilon_w(\varepsilon_m)$ is the dielectric function inside (outside) the wire, $L_i(i = x,y)$ is the edge width of the rectangular wire whose growth direction is along z, and $q_i(i = x,y)$ is the phonon wavevector. We must have,

$$q_x^2 + q_y^2 = q^2 \tag{9a}$$

$$q_x L_x = q_y L_y \tag{9b}$$

where equation 9b is the requirement that potentials of optic phonons in the x and y directions should have the same parity. Neglecting the damping and crystal anisotropy, the dielectric function $\varepsilon_w(\omega)$ can be expressed as,

$$\epsilon(\omega) = \epsilon_\infty \frac{\omega_{LO}^2 - \omega^2}{\omega_{TO}^2 - \omega^2} \tag{10}$$

and the Lyddane-Sachs-Teller (Yu and Cardona, 1999) relation gives

$$\frac{\epsilon_0}{\epsilon_\infty} = \frac{\omega_{LO}^2}{\omega_{TO}^2} \tag{11}$$

where ε_0 and ε_∞ are low and high-frequency values of $\varepsilon(\omega)$, respectively. We can solve for the S and AS mode SO phonon dispersions from equations 1-4:

$$\omega_{SO}^2(q)_S = \omega_{LO}^2 \left| \frac{\epsilon_\infty[\epsilon_0 \tanh(q_i L_i/2) + \epsilon_m]}{\epsilon_0[\epsilon_\infty \tanh(q_i L_i/2) + \epsilon_m]} \right|$$

$$= \omega_{TO}^2 \left[\frac{\epsilon_0 \tanh(q_i L_i/2) + \epsilon_m}{\epsilon_\infty \tanh(q_i L_i/2) + \epsilon_m} \right] \qquad (12)$$

$$\omega_{SO}^2(q)_{AS} = \omega_{LO}^2 \left| \frac{\epsilon_\infty[\epsilon_0 \coth(q_i L_i/2) + \epsilon_m]}{\epsilon_0[\epsilon_\infty \coth(q_i L_i/2) + \epsilon_m]} \right|$$

$$= \omega_{TO}^2 \left[\frac{\epsilon_0 \coth(q_i L_i/2) + \epsilon_m}{\epsilon_\infty \coth(q_i L_i/2) + \epsilon_m} \right] \qquad (13)$$

for nanowires with infinite edge length, i.e. $L\rightarrow\infty$, tanh $(qL/2)\rightarrow1$, and coth $(qL/2)\rightarrow1$; both symmetric (12) and asymmetric modes (13) recover again the SO phonon frequency of an infinite flat semiconductor surface expressed by (5).

2.2.1 ZnS nanowire

High crystalline, rectangular cross-sectional uniaxial wurtzite ZnS nanowires is grown along either *a*-axis ([100]) or the *c* axis ([001]) and details phonon spectra have been discussed by Xiong et al., (2004). The crystal anisotropy and the two growth orientations make the calculations even more complicated. Isotropic equation has been employed to capture the essential physical ideas without too much complication. An exact treatment for the dielectric function and the Lyddane–Sachs–Teller relation for uniaxial wurtzite crystals can be found. For wurtzite ZnS, $\varepsilon_{11}(\infty)$ and $\varepsilon_{33}(\infty)$ vary from 8.25 to 8.76. As an isotropic approximation of ε_0 = 8.3 and ε_∞ = 5.11 from and ω_{LO} = 346.5 cm^{-1} are made.
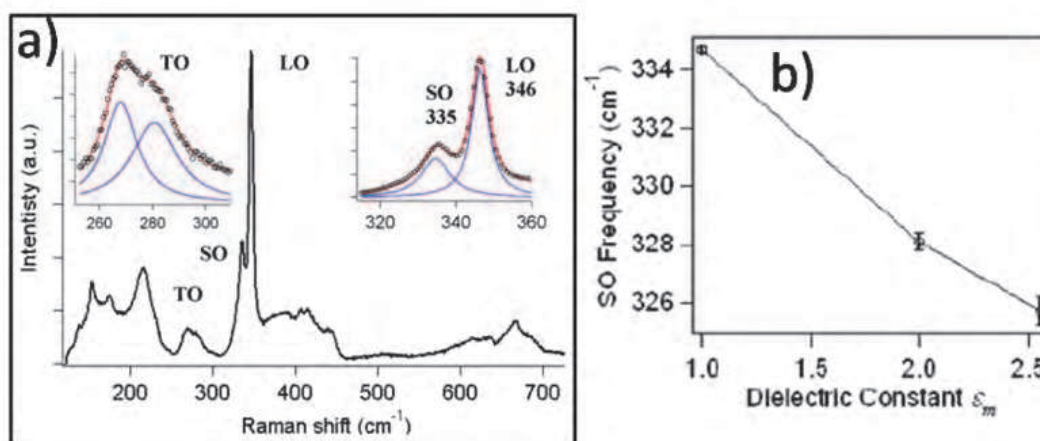

Fig. 16. (a) Raman spectrum of ZnS nanowires collected in air (ε_m=1). Two insets show Lorentzian line shape analysis of LO (346 cm^{-1}) and SO (335 cm^{-1}) modes and TO doublet (269, 282 cm^{-1}), (b) Variation of SO band peak positions as a function of the dielectric constants of the overlaying media. (Xiong et al., 2004 Copyright © American Chemical Society; Applied for permission).

Raman spectrum of rectangular cross section ZnS nanowires collected at room temperature in air is show in figure 16. Strong first-order LO scattering has been observed at 346 cm^{-1} and a TO doublet has been reported at 269 and 282 cm^{-1}. Some broad continuum scattering

intensity has been observed in the range 350–450 cm⁻¹ along with other features due to combination and overtone modes. The insets in figure 16 show the Lorentzian line shape analysis of the TO doublet and the LO–SO bands. Magnified spectrum is shown (Fig. 16) for the line shape analysis of the LO-SO region. As shown in figure 16 an additional Raman band have been reported at 335 cm⁻¹ (in air) for square cross section ZnS nanowires. It has also been identified with SO modes, as it red shifts in dielectric media (dichloromethane and aniline). In air, the SO band found at 335 cm⁻¹ red shifts to 328 cm⁻¹ in dichloromethane and 326 cm⁻¹ in aniline. The variation of experimental SO frequencies ZnS nanowires with the dielectric constants for the surrounding liquids are plotted in figure 16b. A linear decrease of the SO frequency has been reported as the dielectric constant of the overlaying medium is increased.

Figure 17(a) shows the SO dispersions for both S and AS asymmetric modes of ZnS for three overlaying dielectric media (ε_m). The S and AS modes exhibit different dispersion at small qL, but they converge to the same frequency as qL approaches very large values. Three horizontal dashed lines represent the actual experimental SO phonon frequencies in the three dielectric media. The three experimental frequencies connect to approximately the same wave vector q, showing an important self-consistency proof of the validity of the dielectric continuum model (Givargizov et al., 1973; Johansson et al., 2006). The surface modulation in TEM images (inset in Fig. 17a) along the wire axis, however, appears to be not as clearly periodic as in cylindrical nanowires. Nevertheless, still it confirms that the theoretical calculations based on the dielectric continuum model are consistent with TEM images; i.e., the wavelength of the perturbation that breaks the symmetry and activates SO mode is $\lambda \sim 70$ nm.
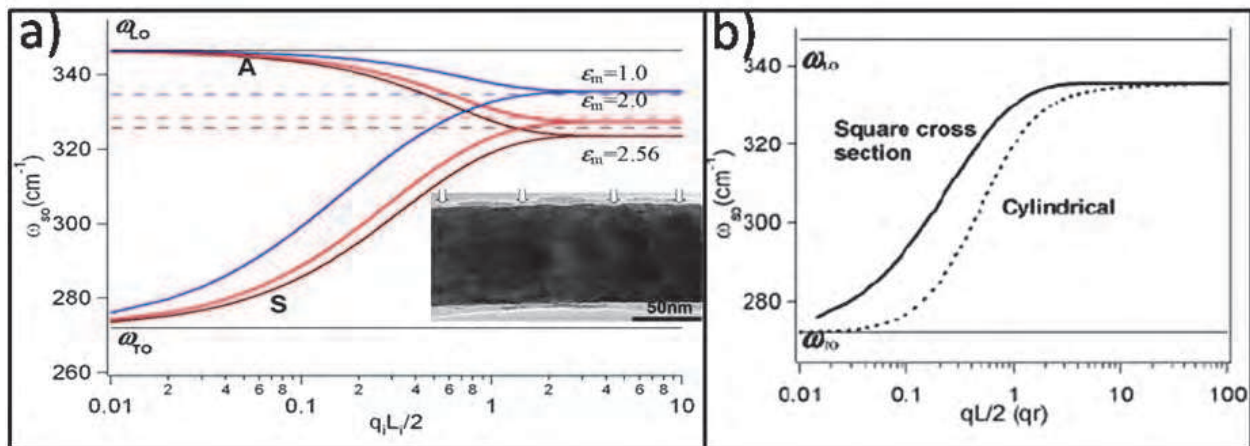

Fig. 17. (a) SO phonon dispersion for rectangular cross section wires for three dielectric media calculated from eqs 12 and 13, corresponding to S and AS modes, respectively. Three dashed lines represent the measured SO frequencies in air (ε_m = 1), dichloromethane (ε_m=2), and aniline (ε_m =2.56). Two horizontal solid lines represent LO and TO frequencies. Inset is the TEM images of ZnS nanowires. The surface modulation along the wire axis is clearly identified. The hollow arrows indicate the position where the minimum takes place; the average distance between the arrows is about 70 nm. (b) Calculated SO dispersions for rectangular wires with square cross sections (solid curve) and a supposed cylindrical ZnS nanowire (dashed curve) with a radius r in air. Two horizontal lines represent the LO and TO phonon branches, assuming they are dispersion less. (Xiong et al., 2004 Copyright © American Chemical Society; Applied for permission).

The effect of the nanowire morphology, looking into the cross-sectional shape, on the SO phonon dispersions has been made by computing the SO mode dispersion for ZnS cylindrical nanowires with diameter (d) against that of square cross section nanowires with sides of length $L = d$. The dashed curve shows the calculated SO dispersion for cylindrical ZnS nanowires in air (Fig. 17b). From the measured SO frequency in air, e.g., ω_{SO} = 334.7 cm^{-1} and using the SO dispersion (Fig. 17a), the important wave vector q responsible for activating the SO modes is estimated. It has been reported that qd = 25 predicts the experimental SO frequency in air. The wavelength for the perturbation is therefore $\lambda = 2\pi/q$ =13 nm. This λ differs by a factor of about 5 from the λ obtained from the rectangular cross section SO analysis. So it is obvious that the correct nanowire shape must be used in the analysis. The importance of the effect of the nanowire shape on the SO analysis is apparent from figure 17b.

2.2.2 GaN nanoribbons

The higher wave number fitted Raman spectrum (Fig. 18a) has been obtained from the GaN nanoribon grown inside the nanochannels of Na-4 in our study (Bhattacharya et al., 2011). The dispersion relation $\omega_{SO}(q)$ for a GaN nanoribbon encapsulated in Na-4 mica (Fig. 18b) shows a plot of both the S and AS modes of SO phonon dispersion curves for A_1 and E_1 symmetries. Horizontal lines corresponding to the experimentally observed wavenumbers at 633 and 678 cm^{-1} intersect the dispersion curves of AS$_{SO}$ modes at $q_i L_i/2$ values (marked with vertical lines). The wavevectors q of the surface perturbation that is responsible for activating the SO modes are estimated with the experimental 633 and 678 cm^{-1} ω_{SO} values (Fig. 18b). We find that $q_i L_i/2$ = 0.16 and 0.63 correspond to A_1 and E_1 symmetries, respectively. In the case of nanostructures, or for that matter on the surface, both even and odd modes of polarization eigen vectors are allowed for the breakdown in translational symmetry. Thus, both AS and S modes can respond to SO phonon modes. In the present study, we find the intersection only with AS mode, which is only incidental.
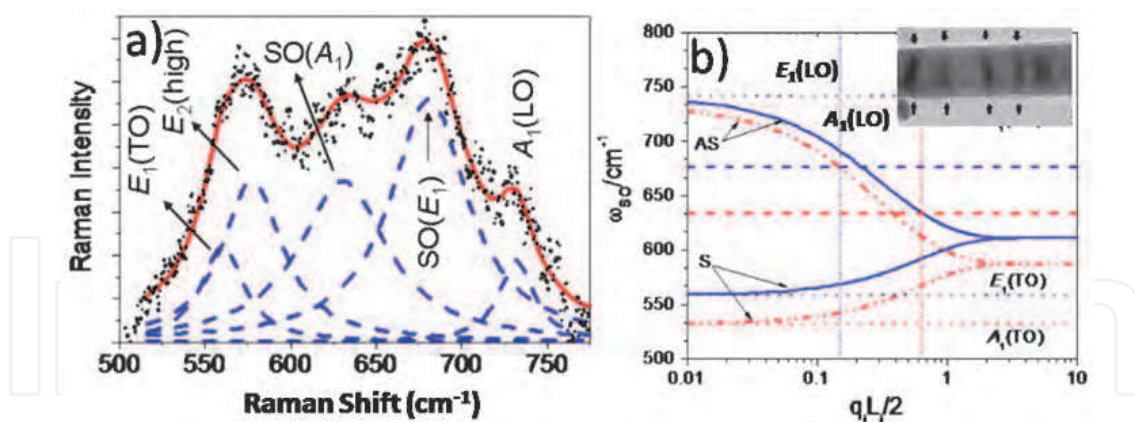

Fig. 18. (a) Higher wave numbers fitted Raman spectra of Na-4 mica–GaN with 325 nm excitation with Lorentzian lineshapes corresponding to various known modes of GaN along with SO modes.(b) SO phonon dispersion curves calculated for Na-4 mica encapsulated GaN nanoribbons (calculated for rectangular cross-section). The continuous and dashed-dot-dot curves correspond to E_1 and A_1 symmetries, respectively. AS and S modes are indicated in the plot. Two dashed horizontal lines represent the experimentally measured SO wavenumbers at 633 and 678 cm^{-1}. Four other horizontal dotted lines represent the LO and TO wavenumbers of bulk GaN corresponding to the E_1 and A_1 symmetries. Inset in figure 18b shows a typical GaN straight nanoribbon (width ~50 nm) with observed surface modulations. (Bhattacharya et al., 2011 Copyright © John Wiley & Sons, Ltd.)

The observed SO phonons intensities are comparable to those of the other phonons. The wavelengths for the SO potential perturbation (with the average nanoribbon cross-section dimensions as 50×1 ($L_x \times L_y$) nm²), that breaks the symmetry and activates the SO mode is $\lambda = 2\pi/q_i$ ($i = x$, y) 20–1000 nm (A_1 symmetry) and 5–250 nm (E_1 symmetry). Surface roughness with a modulation of ~50 nm has been reported (indicated by arrows in the inset of Fig. 18b), and any integral multiple equivalent to the λ (5×50 nm = 250 nm or 20×50 nm = 1000 nm) will be sufficient to initiate breakdown of translational symmetry for the contribution of SO potential to the SO modes.

The interaction potentials for the SO modes scales as $(q_z L_x)^{-1}$ and $(q_z L_y)^{-1}$ resulting in the electron–SO phonon scattering in nanoribbons dominating over electron–LO confined phonon scattering rate for $q_z \ll L_x^{-1}(L_y^{-1})$ (Stroscio et al., 1990). The observed $q_z \approx 2\times10^5-6\times10^4$ cm⁻¹ (λ = 250–1000 nm) $\ll L_y^{-1} \approx 1 \times 10^7$ cm⁻¹ ($L_y \approx 1$ nm) makes the intensity of the SO mode comparable to that of the other optical modes as a result of relatively narrow distribution of surface perturbation in these samples about 50 nm. However, other rigid modes corresponding to even L (quantum number corresponding to axial modes) in the continuum model of the elongated nanostructures contribute to the width of the SO peak (Nobile et al., 2007).

2.3 SO phonons in spheroidal geometry

It is convenient to use cylindrical coordinates ($\rho \theta, \emptyset, z$) for a spheroidal nanorod with semi-axes a and c and the dispersions of the anisotropic dielectric function $\epsilon_\perp(\omega)$ and $\epsilon_z(\omega)$ in the following denotations (Fonoberov & Baladin, 2004, 2005)

$$g_1 = \frac{\epsilon_z(\omega)}{\epsilon_\perp(\omega)}; \quad g_2 = 1; \quad f_n = c^2 - g_n a^2$$

$$p_n = f_n + z^2 + g_n \rho^2; \qquad t_n = \sqrt{p_n^2 - 4f_n z^2}$$

$$\xi_n = |z| \sqrt{\frac{2}{p_n - t_n}}; \quad \eta_n = \text{sign}(z) \sqrt{\frac{p_n - t_n}{2f_n}}$$

the phonon potential inside (in) and outside (out) of the nanorod as

$$V_{L,M,\omega}^{(in)}(\rho, \emptyset, z) = \frac{P_L^M(\xi_1)}{P_L^M(c/\sqrt{f_1})} P_L^M(\eta_1) e^{iM\emptyset} \tag{14}$$

$$V_{L,M,\omega}^{(out)}(\rho, \emptyset, z) = \frac{Q_L^M(\xi_2)}{Q_L^M(c/\sqrt{f_2})} P_L^M(\eta_2) e^{iM\emptyset} \tag{15}$$

Here P_L^M and Q_L^M are associated Legendre functions of the first and second kind, respectively. The integers L (L$\geq$ 1) and M ($|M| \leq L$) are quantum numbers of the phonon mode, and the eigen frequencies ω of the phonon modes (Fonoberov & Baladin; 2005).

2.3.1 CdSe nanorod

The optical phonon excitations of randomly oriented and laterally aligned nanorod arrays (Fig. 19a) have been studied using resonant Raman scattering by Nobile and co-authors (Nobile et al., 2007). Colloidal wurtzite CdSe nanorods are fabricated by chemical synthesis in a hot mixture of surfactants. Nanorods are aligned by drop-caste on to an interdigitated

electrode device and applying an AC electric field of 10^5 V.cm^{-1} at a frequency of 10 MHz during solvent evaporation (Fig. 19b).
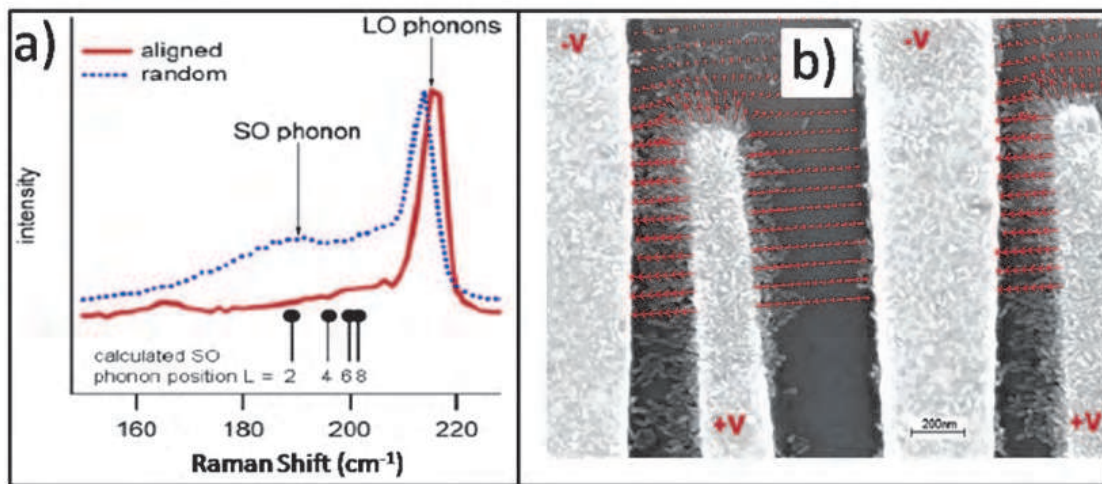

Fig. 19. (a) Resonant Raman spectra of randomly oriented (blue dotted line) and laterally aligned (solid red line) nanorods at T=15 K recorded in parallel polarization with respect to incident and detected light. The black bars indicate the calculated energies for the first four Raman active SO phonon modes. (b) Scanning electron microscope image of laterally aligned nanorods in between interdigitated electrodes defined by electron beam lithography. The red arrows show the calculated electric field for bias $\pm$V applied to neighboring electrodes for alignment. In the lower part of the image, the electric field lines are not shown in order to enhance the visibility of the nanorods. The rods accumulate in the regions of strongest electric field and observe excellent alignment with the electric field. (Nobile et al., 2007 Copyright © American Chemical Society; Applied for permission).

Raman spectra of randomly oriented (dotted) and closely packed laterally aligned (solid) nanorods (diameter 10 nm, and length 50 nm), which are taken on regions outside and within the interdigitated electrodes, respectively, on the same sample are shown in figure 19a. In the spectrum of the randomly oriented rods, the LO phonon at 214 cm^{-1}, and at the low-energy side, a broad peak centered around 185 cm^{-1} originating from the SO phonon modes are observed. The spectrum of the laterally aligned nanorods (with *c*-axis perpendicular to the incident light polarization) shows a very small blue-shift of the LO phonon peak and a significant decrease in the SO phonon intensity. In this contest, the experimental data is compared with first principle calculations of nanorods with corresponding aspect ratio (*c/a* of CdSe nanorods taken around 5). The theory predicts that only phonon modes with even L and with M =0 can be active in a resonant Raman spectrum.

According to the formalism reported above, figure 20 shows the calculated (phenomenological) potential of the SO phonon modes with M = 0 and even angular quantum numbers L. The energy of these modes is depicted in figure 19a by the black bars with full heads (energy increasing with higher angular momentum number). The calculated Raman active energies with the data obtained from the randomly oriented rods have shown excellent agreement. The phonon potentials of the SO modes with low L extend significantly outside of the rod surface as shown in figure 20.
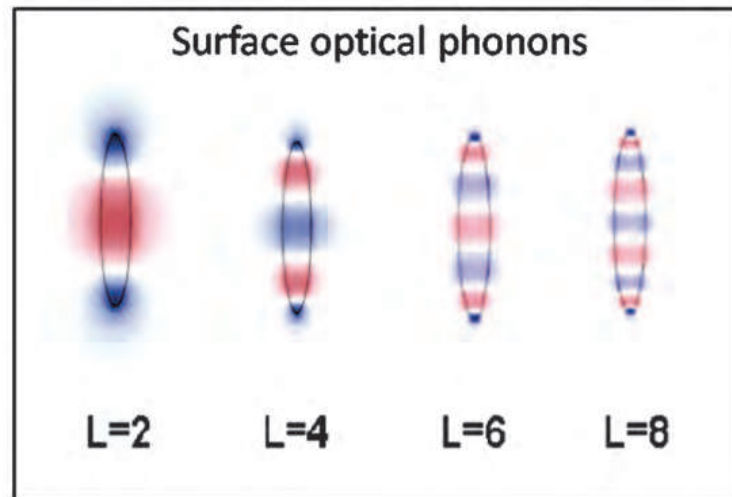
Fig. 20. Cross sections of the calculated phonon potential for the SO modes with $M = 0$ and different angular momentum. Only SO phonon modes with even quantum number L are Raman active. Note that the $L = 2$ mode has significant phonon potential outside the nanorod surface. (Nobile et al., 2007 Copyright © American Chemical Society; Applied for permission).

The SO or interface phonon modes are stimulated by the change in dielectric medium at the interface. In a close-packed 2D array of nanorods, the space adjacent to the rods is occupied by other nanorods. Thus the dielectric medium surrounding the individual rods is severely modified, leading to the observed suppression of the SO phonon modes. The fact that SO phonon modes with higher angular momentum extend less outside the rod region accounts for the low-energy shoulder of the LO phonon peak around 200 cm^{-1}. The observation agrees well with the spatial distribution of potential of the SO phonon modes with long axis orientation of nanowires.

3. Conclusion

The essential for understanding SO phonons is presented in this report for a wide range of compound semiconductor nanowires. The experimental analysis, as well as, theoretical calculations concluded that the SO mode in semiconductor nanowires is primarily associated with the surface modulation and geometry. The SO mode is clearly identified by its shift in the Raman spectrum as the overlaying medium dielectric constant is varied. The characteristic wave length of perturbation of the SO potential can be readily measured by the position of SO mode in Raman spectra. We believe that growth instabilities leading to the appearance of SO modes in the phonon spectra should be a general indicator of the presence of a corrugated surface. The instability of surface modulation mostly arises during vapour-liquid-solid growth of most nanowires system, and strongly depends on growth conditions, such as temperature, impurities, and supersaturation. In general, Raman scattering from SO phonons not only enlighten us on the atomic dynamics on surface but allows also help exploring the interaction of SO phonons with electronic surface states, and hence, can be exploited as a primary tool for surface analysis of one- (nanowire) and two-dimensional systems.

4. Acknowledgement

5. Reference

Adu, K.W.; Xiong Q.; Gutierrez, H.R.; Chen G. & Eklund, P.C. (2006). *Raman Scattering as a Probe of Phonon Confinement and Surface Optical Modes in Semiconducting Nanowires*, Appl. Phys. A 85, 287, ISSN: 0947-8396

Algra, R.E.; Verheijen, M.A.; Borgstrom, M.T.; Feiner, L.F.; Immink, G.; van Enckevort, W.J.P.; Vlieg, E. & Bakkers, E.P.A.M. (2008). *Twinning Superlattice in Indium Phosphide Nanowires*, Nature, 456, 369-372, ISSN: 0028-0836

Arguello, C. A.; Rousseau, D. L.; & Porto, S. P. S. (1969). *First-Order Raman Effect in Wurtzite-Type Crystals,* Phys. Rev. 181, 1351.

Benedek, G. & Toennies, J. P. (1994). *Helium Atom Scattering Spectroscopy of Surface Optical Phonons: Genesis and Achievements*, Surf. Sci., 299/300, 587

Bhattacharya, S.; Datta, Anindya.; Dhara, S. & Chakravorty, D. (2011). *Surface Optical Raman Modes in GaN Nanoribbons*, J. Raman Spectrosc., 42, 429-433 ISSN:1097-4555

Cao, L.; White J. S.; Park J. S.; Schuller J. A.; Clemens B. M. & Brongersma M. L. (2009). *Engineering Light Absorption in Semiconductor Nanowire Devices*, Nat. Mat., 8, 643-647, ISSN: 1476-1122

Cao, L.Y.; Laim, L.; Valenzuela, P. D.; Nabet, B. & Spanier, J.E. (2007). *On the Raman Scattering from Semiconducting Nanowires,* J. Raman. Spectrosc. 38, 697-703, ISSN: 0377-0486

Cao, L.Y.; Nabet, B. & Spanier, J.E. (2006). *Enhanced Raman Scattering from Individual Semiconductor Nanocones and Nanowires*, Phys. Rev. Lett., 96, 157402-5, ISSN: 0031-9007

Falge, H. J.; Borstel, G.; Otto, A. (1974). *Dispersion of Generalized Surface Optical Phonon Polaritons on α-Quartz Observed by Attenuated Total Reflection*, Phys. Stat. Solid B 65, 123

Fonoberov, V. A. & Balandin, A. A. (2004). *Interface and Confined Optical Phonons in Wurtzite Nanocrystals*, Phys. Rev. B 70, 233205.

Fonoberov, V. A. & Balandin, A. A. (2005). *Polar Optical Phonons in Wurtzite Spheroidal Quantum Dots: Theory and Application to ZnO and ZnO/MgZnO Nanostructures*, J. Phys.: Condens. Matter, 17, 1085-1097.

Frechette, J. & Carraro, C. (2006). *Diameter-Dependent Modulation and Polarization Anisotropy in Raman Scattering from Individual Nanowires,* Phys. Rev. B, 74, 2161404, ISSN: 1098-0121

Fuchs, R.; & Kliewer, K. L. (1965). *Optical Modes of Vibration in an Ionic Crystal Slab*, Phys. Rev. 140, A2076

Givargizov, E. I. (1973). *Periodic Instability in Whisker Growth*, J. Cryst. Growth, 20, 217.

Gupta, R.; Xiong, Q.; Mahan, G.D. & Eklund, P.C., (2003). *Surface Optical Phonons in Gallium Phosphide Nanowires*, Nano Lett., 3, 1745, ISSN: 1530-6984

Hartschuh, A.; Pedrosa, H.N.; Novotny, L. & Krauss, T.D. (2003). *Simultaneous fluorescence and Raman scattering from single carbon nanotubes*, Science, 301, 1354-6, ISSN:0036-8075

Hayden, O.; Agarwal, R. & Lu, W. (2008). *Semiconductor Nanowire Devices*, Nanotoday, 3, 12, ISSN:1748 01321

Hsiao, C. L.; Tu, L.W.; Chi, T. W.; Chen, M.; Young, T. F.; Chia, C.T.; Chang, Y. M. (2007). *Micro-Raman Spectroscopy of a Single Freestanding GaN Nanorod Grown by Molecular Beam Epitaxy,* Appl. Phys. Lett. 90, 043102

Ibach, H. & Mills, D. L. (1982). *Electron Energy Loss Spectroscopy and Surface Optical Vibrations,* Academic, New York

Johansson, J.; Karlsson, L.S.; Svensson, C.P.T.; Martensson, T.; Wacaser, B.A.; Deppert, K.; Samuelson, L. & Seifert, W. (2006). *Structural Properties of (111)B -Priented III–V Nanowires,* Nat. Mater. 5, 574

Lin, H.M.; Chen, Y.L.; Yiang, J.; Liu, Y.C.; Yin, K.M.; Kai, J.J.; Chen, L.C.; Chen, Y.F. & Chen, C.C. (2003). *Synthesis and Characterization of Core-Shell GaP@GaN and GaN@GaP Nanowires,* Nano Lett., 3, 4, 537-541, ISSN: 1530-6984

Livneh, T.; Zhang, J.P.; Cheng, G.S. & Moskovits, (2006). *Polarized Raman Scattering from Single GaN Nanowires,* Phys. Rev. B, 74, 035320, ISSN: 1098-0121

Lu, W.; & Lieber, C. M. (2007). *Nanoelectronics from the Bottom Up,* Nat. Mater., 6, 841 - 850 ISSN: 1476-1122

Mahan, G.D.; Gupta, R.; Xiong, Q.; Adu, C.K. & Eklund, P.C., (2003). *Optical Phonons in Polar Semiconductor Nanowires,* Phys. Rev. B, 68, 073402, ISSN: 0163-1829

Nobile, C.; Fonoberov, V. A.; Kudera, S.; Torre, A. D.; Ruffino, A.; Chilla, G.; Kipp, T.; Heitmann, D.; Manna, L.; Cingolani, R.; Balandin, A. A. & Krahne, R. (2007) , *Confined Optical Phonon Modes in Aligned Nanorod Arrays Detected by Resonant Inelastic Light Scattering,* Nano Lett. 7, 476.

Patolsky, F.; Timko, B. P.; Zheng, G.; & Lieber, C. M. (2007). *Nanowire Based Nanoelectronic Devices in the Life Sciences,* MRS Bulletin, 32, 142.

Pauzauskie, P.J., Talaga, D., Seo K., Yang, P.D. & Lagugne-Labarthet F. (2005). *Polarized Raman Confocal Microscopy of Single Gallium Nitride Nanowires,* J.A.C.S., 127, 49, 17146, ISSN: 0002-7863

Pauzauskie, P. J.; & Yang, P. (2006). *Nanowire Photonics,* Materials Today, 9, 36, ISSN:1369 7021

Richter, W.; Hinrichs, K. & Esser, N. (2000). *Raman Scattering from Surface Phonons on Semiconductors,* Proc. Int. Symp. on Progress in Surface Raman Spectroscopy, Editors: Tian, Z.Q.; Ren, B.; Xiamen University Press, S.133-136, ISBN 7-56151629

Sahoo, P.; Dhara, S.; Dash, S.; Tyagi, A.K.; Raj, B.; Das, C.R.; Chandramohan, P.; & Srinivasan, M.P. (2010). *Surface Optical Modes in GaN Nanowires,* Int. J. Nanotechnol., 7, 823-832.

Sahoo , S.; Dhara, S.; Arora, A. K.; Krishnan, R.; Chandramohan, P. & Srinivasan, M. P. (2010). *Raman Scattering from Surface Optical Phonon in Diameter Modulated AlN Nanotips,* Appl. Phys. Lett. 96, 103113

Sahoo, S.; Hu, M. S.; Hsu, C. W.; Wu, C. T.; Chen, K. H.; Chen, L. C.; Arora, A. K. & Dhara, S. (2008). *Surface Optical Raman Modes in InN Nanostructures,* Appl. Phys. Lett. 93, 233116

Sernelius, B.E. (2001). *Surface Optical Modes in Physics,* 1st edn. Wiley-VCH, New York, p. 350

Shan, C.X.; Liu, Z.; Zhang, X.T.; Wong, C.C. & Hark S.K. (2006). *Wurtzite ZnSe Nanowires: Growth, Photoluminescence, and Single-Wire Raman Properties,* Nanotechnology, 17, 5561-4, ISSN: 0957-4484

Spirkoska, D.; Abstreiter, G. & Fontcuberta i Morral A. (2008). *Size and Environment Dependence of Surface Optical Phonon Modes of Gallium Arsenide Nanowires as*

Measured by Raman Spectroscopy, Nanotechnology, 19, 435704, ISSN: 0957-4484. http://iopscience.iop.org/0957-4484/19/43/435704/

Stroscio, M.A.; Dutta, M.; ebrary Inc. (2001). *Phonons in Nanostructures*, Cambridge University Press: Cambridge; New York

Stroscio, M. A.; Kim, K. W.; Littlejohn, M. A.; Chuang, H. H., (1990). *Polarization Eigenvectors of Surface-Optical Phonon Modes in a Rectangular Quantum Wire,* Phys. Rev. B, 42, 1488.

Wallis, R.F. (1994). *Surface Optical Phonons: Theoretical Developments*, Surf. Sci. 299/300, 612

Wang, J.; Gudiksen, M. S.; Duan, X.; Cui, Y. & Lieber, C. M. (2001). *Highly Polarized Photoluminescence and Photodetection from Single Indium Phosphide Nanowires*, Science, 293, 1455-7, ISSN: 0036-8075

Wu, S.E.; Dhara, S.; Hsueh, T.H.; Lai, Y.F.; Wang, C.Y.; & Liu, C.P. (2009). *Surface Optical Phonon Modes in Ternary Aligned Crystalline InGaN/GaN Multiquantum-Well Nanopillar Arrays*, J. Raman Spectrosc., 40, 2044–2049

Xiong, Q.; Chen, G.; Gutierrex, H.R. & Eklund, P.C., (2006). *Raman Scattering Studies of Individual Polar Semiconducting Nanowires: Phonon Splitting and Antenna Effects,* Appl. Phys. A, 85, 299-305, ISSN: 0947-8396

Xiong, Q.; Wang, J.; Reese, O.; Yoon, L. C. & Eklund, P.C. (2004). *Raman Scattering from Surface Optical Phonons in Rectangular Cross-Sectional w-ZnS Nanowires*, Nano Lett. , 4, 10, 1991-6, ISSN: 1530-6984

Yang, P.; Yan, R. & Fardy, M. (2010). *Semiconductor Nanowire: What's Next?,* Nano letter, 10, 1529-36

Yu, P. Y.; Cardona, M. (1999). *Fundamentals of Semiconductors: Physics and Materials Properties*, Springer, Berlin; New York.

Zardo, I.; Conesa-Boj S.; Peiro F.; Morante, J.R.; Arbiol, J.; Abstreiter, G. & Fontcuberta i Morral A. (2009). *Raman Spectroscopy of Wurtzite and Zinc-Blende GaAs Nanowires: Polarization Dependence, Selection Rules and Strain Effects,* Phys. Rev. B, 80, 245324

Zeng, H.; Cai, W.; Cao, B.; Hu, J.; Li, Y. & Liu P. (2006). *Surface Optical Phonon Raman Scattering in Zn/ZnO Core-Shell Structured Nanoparticles*, Appl. Phys. Lett., 88, 181905, ISSN: 0003-6951.
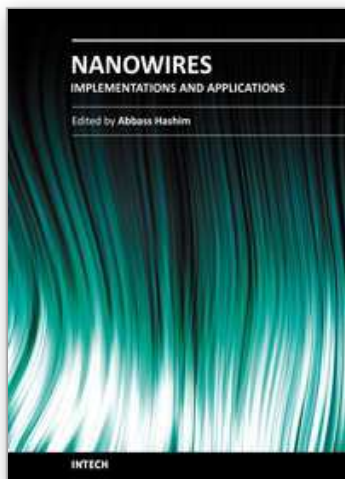
Nanowires - Implementations and Applications
Edited by Dr. Abbass Hashim

This potentially unique work offers various approaches on the implementation of nanowires. As it is widely known, nanotechnology presents the control of matter at the nanoscale and nanodimensions within few nanometers, whereas this exclusive phenomenon enables us to determine novel applications. This book presents an overview of recent and current nanowire application and implementation research worldwide. We examine methods of nanowire synthesis, types of materials used, and applications associated with nanowire research. Wide surveys of global activities in nanowire research are presented, as well.

How to reference

In order to correctly reference this scholarly work, feel free to copy and paste the following:

Prasana Sahoo, A. K. Tyagi, Baldev Raj and S. Dhara (2011). Surface Optical Modes in Semiconductor Nanowires, Nanowires - Implementations and Applications, Dr. Abbass Hashim (Ed.), ISBN: 978-953-307-318-7, InTech, Available from: http://www.intechopen.com/books/nanowires-implementations-and-applications/surface-optical-modes-in-semiconductor-nanowires

INTECH
open science | open minds